Journal of
Medicinal Chemistry



Article

# Structure-Based Bioisosterism Yields HIV 1 NNRTIs with Improved Drug Resistance Profiles and Favorable Pharmacokinetic Properties

Dongwei Kang, Da Feng, Yanying Sun, Zengjun Fang, Fenju Wei, Erik De Clercq, Christophe Pannecouque, Xinyong Liu, and Peng Zhan

*J. Med. Chem.*, **Just Accepted Manuscript** • Publication Date (Web): 15 Apr 2020



## Just Accepted



is published by the American Chemical Society. 1155 Sixteenth Street N.W., Washington, DC 20036

# Structure-Based Bioisosterism Yields HIV-1 NNRTIs with Improved Drug Resistance Profiles and Favorable Pharmacokinetic Properties

Dongwei Kang,[†, &] Da Feng,[†] Yanying Sun,[†] Zengjun Fang,[†, |] Fenju Wei, [†]

Erik De Clercq, [§] Christophe Pannecouque, [§,*] Xinyong Liu[†,&,*] and Peng Zhan,[†, &,*]

[†] *Department of Medicinal Chemistry, Key Laboratory of Chemical Biology (Ministry of Education), School of Pharmaceutical Sciences, Shandong University, 44 West Culture Road, 250012 Jinan, Shandong, P.R. China*

[§] *Rega Institute for Medical Research, Laboratory of Virology and Chemotherapy, K.U. Leuven, Herestraat 49 Postbus 1043 (09.A097), B-3000 Leuven, Belgium.*

[&] *China-Belgium Collaborative Research Center for Innovative Antiviral Drugs of Shandong Province, 44 West Culture Road, 250012 Jinan, Shandong, PR China*

[|] *The Second Hospital of Shandong University, No. 247 Beiyuan Avenue, Jinan 250033, Shandong, P.R. China*

**Abstract**

The development of efficacious NNRTIs for AIDS therapy commonly encountered the rapid generation of drug-resistant mutations, which becomes a major impediment to effective anti-HIV treatment. Using a structure-based bioisosterism strategy, a series of piperidine-substituted thiophene[2,3-*d*]pyrimidine derivatives were designed and synthesized. Compound **9a** yielded the greatest potency, exhibiting significantly better anti-HIV-1 activity than ETR against all of the tested NNRTI-resistant HIV-1 strain. In addition, the phenotypic (cross)-resistance of **9a** and other NRTIs to the different selected HIV-1 strains were evaluated. As expected, no

phenotypic cross-resistance against the NRTIs (AZT and PMPA) were observed with the mutant strains $9a^{res}$ strain. Furthermore, **9a** was identified with improved solubility, lower CYP liability and hERG inhibition. Remarkably, **9a** exhibited optimal pharmacokinetic properties in rats ($F$ = 37.06 %) and safety in mice ($LD_{50}$ > 2000 mg/kg), which highlights **9a** as a promising anti-HIV-1 drug candidate.

**Key Words:** HIV-1; NNRTIs; Thiophene[2,3-d]pyrimidine; Drug Resistance Profiles

## Introduction

According to the Joint United Nations Program on HIV/AIDS (UNAIDS) report 2017, more than 36.9 million people are today living with HIV, including 1.8 million people newly infected in 2017[1]. Human immunodeficiency virus (HIV) infection is now becoming more pandemic. Therefore, the development of efficacious and potent HIV therapeutics has nowadays become an increasingly important goal[2]. The HIV-1 reverse transcriptase (HIV-1 RT) has been considered as one of the most attractive targets for developing novel anti-HIV drugs for its essential role to transcribe single-stranded RNA into double-stranded DNA in the life cycle of HIV-1[3]. RT inhibitors could be divided into nucleoside reverse transcriptase inhibitors (NRTIs) and non-nucleoside reverse transcriptase inhibitors (NNRTIs). Among them, NNRTIs has gained an increasingly important role in highly active antiretroviral therapy (HAART) regimens used to treat AIDS patients for their potent antiviral activity, high selectivity, and lack of mitochondrial toxicity which characterizes the NRTIs. Up to now, more than 50 structurally diverse classes of compounds have been reported as NNRTIs, including diarylpyrimidine (DAPY)[4-7],

dihydroalkyloxy-benzyl-oxopyrimidine (DABO)[8], 1-[(2-hydroxyethoxy) methyl]-6-(phenylthio)thymine (HEPT)[9], and indolylarylsulfone (IAS)[10]. Among them, six NNRTIs have been approved by the US FDA for HIV-1 treatment, including the first generation NNRTIs nevirapine (NVP), delavirdine (DLV), efavirenz (EFV) and the second generation NNRTIs etravirine (ETR), rilpivirine (RPV), and doravirine (DOR)[1]. Although they have achieved great success in the treatment of HIV-1 patients, drug-resistant mutants rapidly emerge with their clinical application because of their allosteric mechanism of action and low genetic barrier[11], for example, L100I, K103N and Y181C for the first generation NNRTIs, RES056 for ETR, Y181C and E138K for RPV, V106A, F227L and L234I for DOR[12].

With ETR and RPV as lead compounds, our previous efforts have led to the design and synthesis of two piperidine-substituted thiophene[3,2-*d*]pyrimidine NNRTIs **K-5a2** and **25a** (**Figure 1**)[13, 14]. Both compounds feature a thiophene[3,2-*d*]pyrimidine central ring, keeping the 4-cyano-2,6-dimethylphenyl and 4-cyanovinyl-2,6-dimethylphenyl structures in the left wing of ETR of RPV, while replacing their cyanophenyl right wing with a piperidine-linked benzenesulfonamide group. Compared with ETR and RPV, both compounds exhibited increased anti-HIV-1 potency against wild-type (WT) virus and virus strains with a variety of NNRTI-resistant mutations. Especially compound **25a** afforded 3-4-fold improvement of *in vitro* antiviral potency against WT, L100I, K103N, Y181C, Y188L, E138K and RES056 (K103N+Y181C), and 10-fold improvement against F227L+V106A relative to ETR. However, both compounds suffered from a stronger human ether-à-go-go

related gene (hERG) inhibitory activity (**K-5a2**, $IC_{50}$ = 0.130 μM; **25a**, $IC_{50}$ = 0.186 μM). In addition, **25a** showed a higher cytotoxicity ($CC_{50}$ = 2.30 μM) and lower bioavailability (*F* = 16.19 %). Therefore, further structure modification is still needed to achieve improved antiviral potency, decreased toxicity and favorable pharmacokinetic properties.

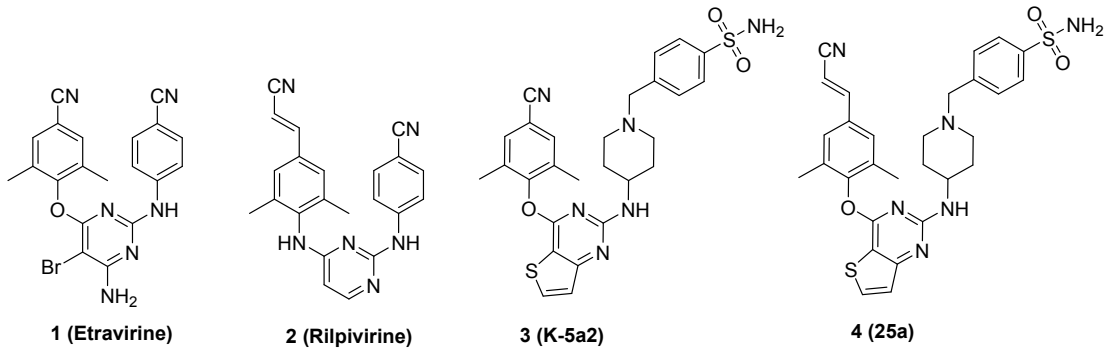


**Figure 1**. Chemical structures of U.S. FDA approved NNRTI drugs and our previously reported thiophene[3,2-*d*]pyrimidine leads **3** (**K-5a2**) and **4** (**25a**).

To seek valuable insights into the favorable structural features of **K-5a2** and **25a** and give insight for designing novel NNRTIs with improved drug resistance profiles, the co-crystal structures of HIV-1 RT in complex with the two inhibitors were determined in our previous study[15]. These high-resolution structures illustrate the structural flexibility of the inhibitors, extensive hydrophobic interactions and the network of main chain hydrogen bonds with NNRTIs binding pocket (NNIBP) accounts for their increased activity against resistance-associated variants (**Figure 2**). Especially, the newly fused thiophene ring could develop novel interaction with Glu138 through a water-mediated hydrogen bond, which was different from our previous reported DAPY NNRTIs[16, 17]. In the current study, with **25a** as lead and keep its privileged left wing unchanged, the bioisosterism strategy was used to design

thiophene[2,3-*d*]pyrimidine replacements for the thiophene[3,2-*d*]pyrimidine central ring of **25a**[18], with the hope that the thiophene ring could establish novel hydrogen bond with the backbone of Lys101 (**Figure 2**). Moreover, six different aryl substituents containing hydrogen bond donor and acceptor were introduced to the piperidin-4-yl-amino moiety of the right wing. Their activity against WT and resistant strains at the cellular and enzymatic level has been investigated. Then, we also studied the development of antiviral resistance to the most potent inhibitor **9a**, the leads **K-5a2** and **25a** by growing HIV-1 strains in the presence of increasing drug concentration and determined its phenotypic cross-resistance. Furthermore, its cytochrome P450 proteins (CYP450) and hERG inhibitory activity, pharmacokinetics and acute toxicity also evaluated detailed.

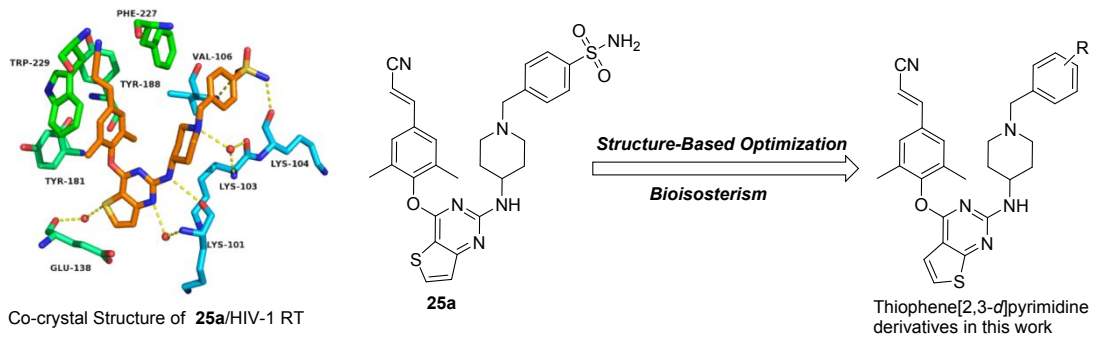


**Figure 2**. Structure-based bioisosterism yields thiophene[2,3-d]pyrimidine derivatives.

## CHEMISTRY

The synthetic protocol for the novel designed derivatives is outlined in **Scheme 1**. The commercially available 2,4-dichlorothiophene[2,3-*d*]pyrimidine (**5**) was selected as starting material, which was treated with 3,5-dimethyl-4-hydroxybenzaldehyde afforded intermediate **6**. The cyanovinyl

compound **7** was obtained by reaction of **6** with diethyl cyanomethylphosphonate under Wittig-Horner reaction. Then **7** was treated with *N*-(*tert*-butoxycarbonyl)-4-aminopiperidine and trifluoroacetic acid to yield the key intermediate **8**, which was reacted with substituted benzyl chloride (or bromide) to give the target compounds **9a-f**. All novel target compounds were fully characterized by electrospray ionization mass spectrometry (ESI-MS), proton nuclear magnetic resonance spectroscopy ($^{1}$H NMR) and carbon nuclear magnetic resonance spectroscopy ($^{13}$C NMR). The purity of all target compounds was > 95% as determined by analytical HPLC.

**Scheme 1. Synthesis of 9a-f[a]**

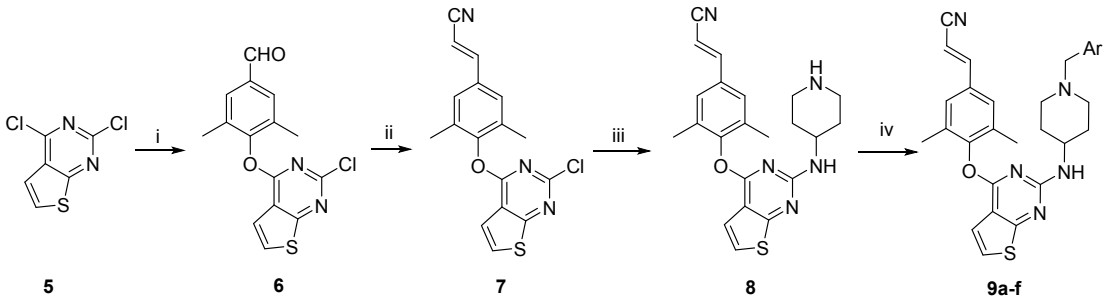


[a] **Reagents and conditions:** (i) 3,5-dimethyl-4-hydroxybenzaldehyde, DMF, $K_2CO_3$, r.t.; (ii) $(EtO)_2P(O)CH_2CN$, *t*-BuOK, THF/DCM, 0°C to r.t.; (iii) 4-(*tert*-butoxycarbonyl)aminopiperidine, DMF, $K_2CO_3$, reflux; then TFA, DCM, r.t.; (iv) substituted benzyl chloride (or bromide), DMF, $K_2CO_3$, r.t.

## RESULTS AND DISCUSSION

Firstly, the compounds' antiviral activity was evaluated in MT-4 cell cultures infected with wild-type HIV-1 strain ($III_B$) and the most challenging double-mutant strain K103N+Y181C (RES056). The lead compound **25a** was selected as the reference, ETR and RPV were selected as control drugs. The values of $EC_{50}$

(anti-HIV activity), $CC_{50}$ (cytotoxicity) and SI (selectivity index, $CC_{50}/EC_{50}$ ratio) of the target compounds are depicted in **Table 1**.

**Table 1.** Anti-HIV activity, cytotoxicity and SI of target compounds **9a-f**.

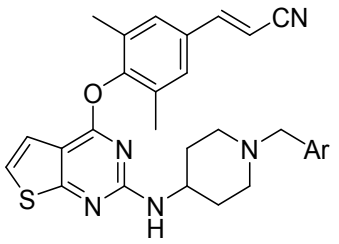


**9a-f**

| Compds | Ar | $EC_{50}$ (nM)[a] | | $CC_{50}$ (μM)[b] | SI[c] | |
|---|---|---|---|---|---|---|
| | | IIIB | RES056 | | IIIB | RES056 |
| **9a** | 4-$SO_2NH_2$-Ph | 3.24±2.15 | 6.45±0.49 | 10.1±3.28 | 3122 | 1569 |
| **9b** | 4-$CONH_2$-Ph | 5.92±2.18 | 66.9±30.2 | 3.54±0.21 | 597 | 53 |
| **9c** | 3-$CONH_2$-Ph | 5.73±0.98 | 62.0±16.3 | 3.95±0.31 | 689 | 64 |
| **9d** | 4-$CO_2C_2H_5$-Ph | 10.6±1.59 | 153±17.6 | 111±18.4 | 10538 | 728 |
| **9e** | 4-F-Ph | 19.7±2.17 | 150±7.01 | 5.84±3.25 | 279 | 39 |
| **9f** | 4-CN-Ph | 12.4±1.71 | 138±15.13 | 7.74±4.61 | 625 | 56 |
| **25a** | | 1.22±0.26 | 5.50±0.81 | 2.30±0.46 | 1882 | 419 |
| **ETR** | - | 4.07±0.149 | 17.0±1.78 | >4.59 | >1128 | >270 |
| **RPV** | - | 1.00±0.27 | 10.7±7.96 | 3.98 | 3989 | 371 |

[a] $EC_{50}$: concentration of compound required to achieve 50% protection of MT-4 cell cultures against HIV-1-induced cytopathicity, as determined by the MTT method.

[b] $CC_{50}$: concentration required to reduce the viability of mock-infected cell cultures by 50%, as determined by the MTT method.

[c] SI: selectivity index, the ratio of $CC_{50}/EC_{50}$.

As depicted in **Table 1**, **9a**, **9b** and **9c** were potent inhibitors of WT HIV-1 ($III_B$) with $EC_{50}$ values of 3.24, 5.92 and 5.73 nM, with comparable activity to the approved drug ETR ($EC_{50}$ = 4.07 nM). Among them, **9a** ($EC_{50}$ = 3.24 nM) yielded the most

active potency, although it was slightly inferior to the lead **25a** ($EC_{50}$ = 1.22 nM) and RPV ($EC_{50}$ = 1.00 nM). However, **9a** proved to be a powerful inhibitor against the mutant HIV-1 strain RES056 with an $EC_{50}$ value of 6.45 nM, that is about 3.0-fold more potent than ETR ($EC_{50}$ = 17.0 nM), and comparable to **25a** ($EC_{50}$ = 5.50 nM) and RPV ($EC_{50}$ = 10.7 nM). More importantly, **9a** displayed much lower cytotoxicity ($CC_{50}$ = 10.1 μM) and higher SI values (SI = 3122 and 1569, respectively) compared to **25a** ($EC_{50}$ = 2.30 μM; SI = 1882 and 419) and RPV ($EC_{50}$ = 3.98 μM; SI = 3989 and 371), which thus achieved our goal of reducing the cytotoxicity. Replacement of the *para*-$SO_2NH_2$ group in the benzene ring of **9a** with *para*-$CONH_2$, *meta*-$CONH_2$, *para*-$CO_2Et$, *para*-F and *para*-CN groups led to a sharply decreased potency to RES056 (**9b-f**, $EC_{50}$ = 62.0-153 nM).

**Table 2.** Activity against mutant HIV-1 strains

| Compds | $EC_{50}$ (nM)[a] | | | | | |
|---|---|---|---|---|---|---|
| | **L100I** | **K103N** | **Y181C** | **Y188L** | **E138K** | **F227L+V106A** |
| **9a** | 2.05±0.58 | 2.34±0.82 | 6.57±0.33 | 7.59±0.46 | 6.70±0.49 | 4.81±0.84 |
| **9b** | 6.11±0.39 | 4.99±0.13 | 12.8±6.97 | 27.1±1.83 | 9.24±0.06 | 15.1±5.71 |
| **9c** | 5.75±0.90 | 5.45±0.80 | 17.7±2.58 | 39.5±4.59 | 18.4±5.26 | 12.2±0.19 |
| **9d** | 19.4±11.2 | 12.0±1.48 | 30.9±0.99 | 120±3.86 | 33.1±1.12 | 32.1±4.73 |
| **9e** | 30.4±2.75 | 22.6±5.81 | 36.3±8.95 | 152±30.0 | 123±34.6 | 127±3.99 |
| **9f** | 21.3±16.6 | 17.3±13.1 | 32.8±0.95 | 117±28.3 | 36.3±0.54 | 32.6±6.93 |
| **25a** | 1.34±0.50 | 0.96±0.07 | 5.00±0.11 | 5.45±0.20 | 4.74±0.160 | 2.70±1.74 |
| **ETR** | 5.38±2.06 | 2.35±0.67 | 15.7±2.12 | 20.5±2.92 | 14.4±2.27 | 29.4±7.79 |
| **RPV** | 1.54±0.00 | 1.31±0.36 | 4.73±0.48 | 79.4±0.77 | 5.75±0.11 | 81.6±21.2 |

[a] $EC_{50}$: concentration of compound required to achieve 50% protection of MT-4 cell cultures against HIV-1-induced cytopathicity, as determined by the MTT method.

Furthermore, all the novel target compounds were evaluated for their activity

against a panel of NNRTIs-resistant single-mutant strains L100I, K103N, Y181C, Y188L, and E138K, as well as the double-mutant strain F227L+V106A. As depicted in **Table 2**, the most promising HIV-1 IIIB inhibitor **9a** also exhibited the highest activity against all mutant strains with single-figure-nanomolar $EC_{50}$ values ranging from 2.05 to 7.59 nM, similar to its activity against WT HIV-1 strain ($EC_{50}$ = 3.24 nM). **Figure 3** provided the comparative activity of **9a**, **25a**, ETR and RPV. As for mutant strains L100I and K103N, all the four compounds exhibited potent activity and have no big difference in their $EC_{50}$ values. Against Y181C and E138K, **9a**, **25a**, and RPV displayed greater potency than ETR. In the case of Y181L and V106A+F227L, RPV exhibited sharply decreased activity ($EC_{50}$ = 79.4 and 81.6 nM, respectively) compared to **9a** ($EC_{50}$ = 7.59 and 4.81 nM) and the lead **25a** ($EC_{50}$ = 5.45 and 2.70 nM). In addition, compounds **9b** and **9c** also demonstrated improved potency against Y181L and V106A+F227L compared to that of RPV. In summary, the data suggested that the novel designed compound **9a** had improved drug resistance profiles over the second-generation NNRTI drugs ETR and RPV, being comparable to that of the lead **25a**.

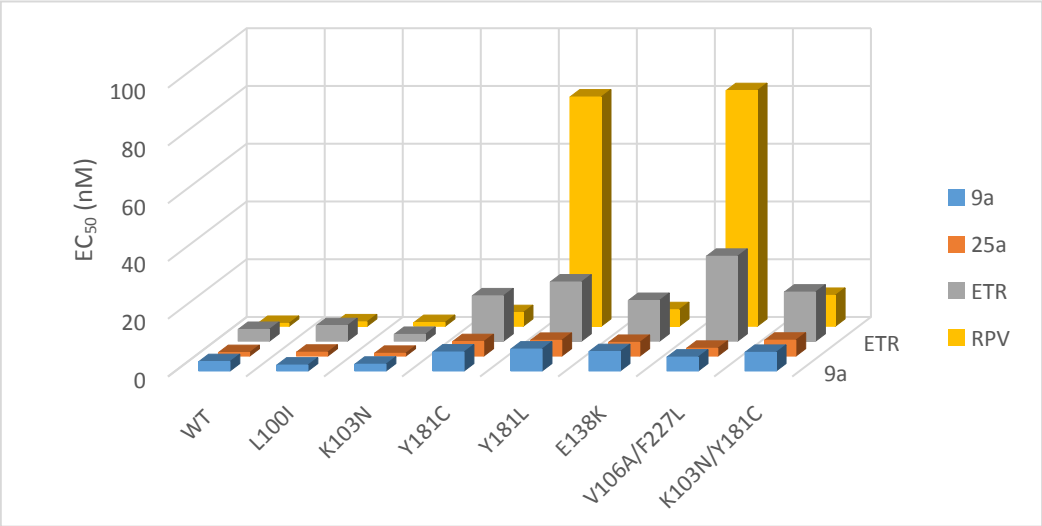


**Figure 3**. Comparison of *in vitro* anti-HIV-1 activities of **9a**, **25a**, ETR and RPV

**Table 3.** SI and RF Values of **9a, 25a, ETR** and **RPV**

| Compds | SI (RF)[a] | | | | | |
|---|---|---|---|---|---|---|
| | **L100I** | **K103N** | **Y181C** | **Y188L** | **E138K** | **F227L+V106A** |
| **9a** | 4926 (0.6) | 4326 (0.7) | 1541 (2.0) | 1334 (2.4) | 1511 (2.1) | 2104 (1.5) |
| **25a** | 1723 (1.1) | 2411 (0.8) | 461 (4.1) | 424 (4.4) | 487 (3.9) | 854 (2.2) |
| **ETR** | >755 (1.1) | >1379 (0.6) | >315 (2.3) | >225 (3.3) | >471 (1.6) | >233 (3.2) |
| **RPV** | 2575 (1.5) | 3045 (1.3) | 841 (4.7) | 50 (80) | 692 (5.8) | 49 (82) |

[a] RF is the ratio of $EC_{50(\text{resistant viral strain})}/EC_{50(\text{wild-type viral strain})}$.

Moreover, SI and fold resistance (RF, ratio of $EC_{50}$ against mutant strain/$EC_{50}$ against WT strain) values of **9a**, **25a**, ETR and RPV were summarized and compared in **Table 3**. Since **9a** had lower cytotoxicity, it displayed much higher SI values toward all the tested mutant strains than did **25a**. More interestingly, **9a** exhibited higher anti-resistance profiles (RF = 0.6 - 2.4) compared to the led **25a**, ETR and RPV. Especially, it displayed more potent activity against L100I (RF = 0.6) and K103N (RF = 0.7) than against HIV-1 $III_B$.

**Selection of HIV-1 ($III_B$) mutant strains under selective pressure**.

To gain further insight into the understanding of the antiviral resistance to the

leads and the novel discovered thiophene[2,3-*d*]pyrimidine analogue **9a**, we passaged the HIV-1 ($III_B$) in cell culture and selected HIV strains resistant to **K-5a2**, **25a** and **9a**. HIV-1 strains resistant to them were generated in MT-4 cells by passaging the virus in the presence of increasing concentrations of the three compounds, respectively. In a control experiment, HIV-1 ($III_B$) was cultured in the absence of any selective drug pressure. After 30 passages, the mutant viruses were harvested at final compound concentrations of 275 nM, 260 nM and 870 nM of **K-5a2**, **25a** and **9a**, respectively (**Figure 4**).

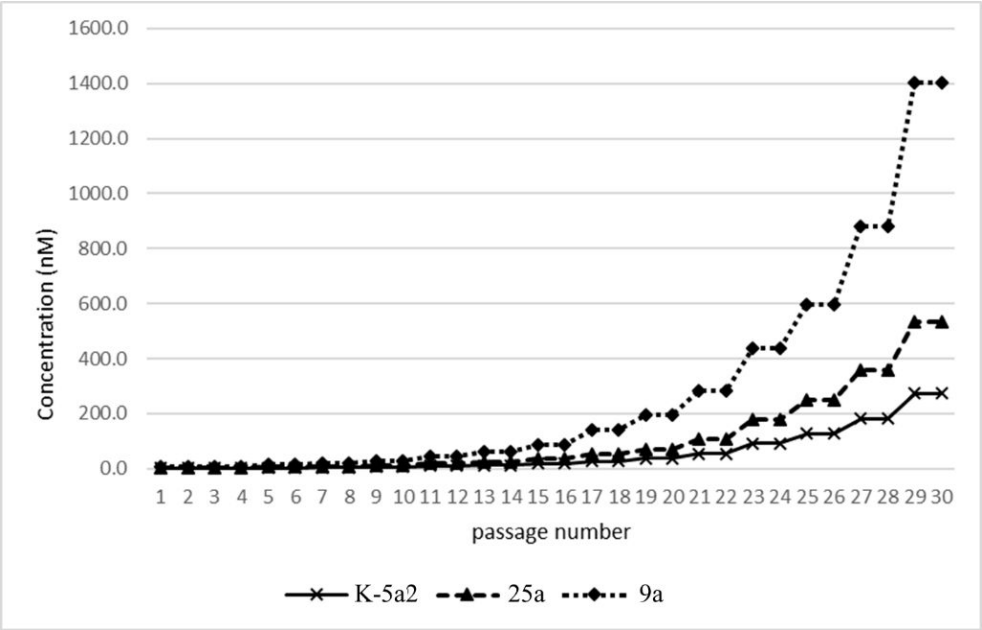


**Figure 4**. Kinetics of resistance development for HIV-1 ($III_B$) following selective pressure with compounds **K-5a2**, **25a** and **9a**. HIV-1 ($III_B$) was cultured in MT-4 cells for 30 passages in the presence of increasing compound concentrations.

**Progressive accumulation of mutations in the RT genes of selected HIV-1 strains.**

Proviral DNA of drug-resistant viruses were isolated and sequenced. Several mutations were detected in the RT gene in comparison with the DNA sequence of the WT HIV-1 ($III_B$) strain, which are summarized in **Table 4**. HIV-1($III_B$) strains

selected during 30 passages in the presence of **K-5a2**, **25a** and **9a** are referred to as K-5a2$^{res}$ strain, 25a$^{res}$ strain, and 9a$^{res}$ strain, respectively. After 30 passages, the Y181C mutation was the most common and present in the whole virus population. In addition, K-5a2$^{res}$ strain contained L100I and V179D, 25a$^{res}$ strain contained V106I and V179D, 9a$^{res}$ strain contained K101E, V108I, F227C and M230I.

**Table 4**: Mutations in the RT of wild-type HIV-1 III$_B$, K-5a2$^{res}$ strain, 25a$^{res}$ strain, and 9a$^{res}$ strain

| Amino Acid | III$_B$ Wild-Type strain | | 9a$^{res}$ Strain | | K-5a2$^{res}$ Strain | | 25a$^{res}$ Strain | |
|---|---|---|---|---|---|---|---|---|
| position | Codon | Amino Acid | Codon | Amino Acid | Codon | Amino Acid | Codon | Amino Acid |
| 100 | TTA | L | TTA | L | ATA | I | TTA | L |
| 101 | AAA | K | GAA | E | AAA | K | AAA | K |
| 106 | GTA | V | GTA | V | GTA | V | ATA | I |
| 108 | GTA | V | ATA | I | GTA | V | GTA | V |
| 179 | GTT | V | GTT | V | GAT | D | GAT | D |
| 181 | TAT | Y | TGT | C | TGT | C | TGT | C |
| 227 | TTC | F | TGC | C | TTC | F | TTC | F |
| 230 | ATG | M | ATA | I | ATG | M | ATG | M |

**Evaluation of phenotypic (cross)-resistance of the different selected HIV-1 strains.**

**Table 5.** Activity against K-5a2$^{res}$ strain, 25a$^{res}$ strain, and 9a$^{res}$ strain

| Compds | EC$_{50}$ (µM)$^a$ (FR)$^b$ | | | |
|---|---|---|---|---|
| | III$_B$ | III$_B$/9a$^{res}$ strain | III$_B$/K-5a2$^{res}$ strain | III$_B$/25a$^{res}$ strain |
| **9a** | 0.0041±0.0015 | 3.60±0.48 (888) | 1.78±1.05 (440) | 0.87±0.26 (214) |
| **K-5a2** | 0.0011±0.0006 | >36.4 (>33333) | >36.4 (>33333) | >36.4 (>33333) |
| **25a** | 0.0027±0.0011 | >5.53 (>2027) | 0.86±0.11 (317) | 1.22±0.01 (450) |
| **NVP** | 0.0879±0.0023 | 3.76±0.45 (43) | >9.51 (>108) | >9.51 (>108) |
| **EFV** | 0.0016±0.0001 | 3.17±0.37 (1881) | 2.03±0.63 (1206) | 1.56±0.28 (925) |
| **ETR** | 0.0027±0.0002 | 1.24±0.10 (450) | 0.53±0.06 (194) | 0.37±0.08 (136) |

| | | | | |
|---|---|---|---|---|
| **RPV** | 0.0009±0.0001 | >3.87 (>4260) | 0.09±0.06 (106) | 0.06±0.01 (68) |
| **AZT** | 0.0127±0.0029 | 0.0010±0.0002 (0.1) | 0.0051±0.0005 (0.4) | 0.0049±0.0005 (0.4) |
| **PMPA** | 4.14±0.18 | 2.17±0.92 (0.5) | 3.76±0.03 (0.9) | 3.31±0.36 (0.8) |

[a] 50% effective concentration or concentration required to inhibit the CPE of different HIV strains by 50% in MT-4 cells.

[b] Increase in 50% effective concentration of the compound against the *in vitro*-selected HIV-1($III_B$) or recombined selected strain compared with the $EC_{50}$ of the compound against the parental HIV-1($III_B$) strain.

To corroborate that the HIV strains selected to grow in the presence of **9a**, **K-5a2**, and **25a** were indeed drug resistant, we determined their antiviral activity against the selected strains in MT-4 cells. In parallel, the first generation NNRTIs NVP and EFV, the second generation NNRTIs ETR and RPV, and nucleoside reverse transcriptase inhibitors (NRTIs) zidovudine (AZT) and tenofovir (PMPA) were determined as well. Notably, the $EC_{50}$ values of the test compounds (**Table 5**) were different from the $EC_{50}$ values displayed in **Table 1**, which may be due to differences in MOI (average number of infectious HIV-1 particles per cell) and has no effect on the whole experimental results. The activities of **K-5a2**, **25a** and **9a** against K-5a2$^{res}$ strain, 25a$^{res}$ strain, and 9a$^{res}$ strain sharply decreased compared to their activity against HIV-1 $III_B$. HIV-1 $III_B$ selected for 30 passages in the presence of **K-5a2**, **25a** and **9a** displayed about >33333, 450 and 888-fold resistance against **K-5a2**, **25a** and **9a**, respectively. In addition, **9a** exhibited modest activity against K-5a2$^{res}$ strain, 25a$^{res}$ strain, and 9a$^{res}$ strain ($EC_{50}$ = 0.87-3.60 μM), while **K-5a2** and **25a** lost their potency toward the 9a$^{res}$ strain. The mutant K-5a2$^{res}$ strain, 25a$^{res}$ strain, and 9a$^{res}$ strain also exhibited stronger resistance against the first and second generation

NNRTIs, including NVP, EFV, ETR and RPV.

Interestingly, no phenotypic cross-resistance against the NRTIs (AZT and PMPA) were observed with the mutant strains K-5a2$^{res}$ strain, 25a$^{res}$ strain, and 9a$^{res}$ strain. Notably, AZT exhibited significantly higher potency against the 9a$^{res}$ strain ($EC_{50}$ = 0.0010 μM), K-5a2$^{res}$ strain ($EC_{50}$ = 0.0051 μM) and 25a$^{res}$ strain ($EC_{50}$ = 0.0049 μM) than against HIV-1 $III_B$ ($EC_{50}$ = 0.0127 μM), with RF values of 0.1, 0.4 and 0.4, respectively. As for PMPA, it also exhibited more potent activity against 9a$^{res}$ ($EC_{50}$ = 2.17 μM), K-5a2$^{res}$ strain ($EC_{50}$ = 3.76 μM) and 25a$^{res}$ strain ($EC_{50}$ = 3.31 μM) than against HIV-1 $III_B$ ($EC_{50}$ = 4.14 μM), with RF values of 0.5, 0.9 and 0.8, respectively. The distinct antiviral resistance profiles of the novel discovered NNRTIs **9a** and the approved NRTIs support the use of them together in HAART and should be helpful in the development of next generation of anti-HIV therapy with an increased genetic barrier to resistance.

**Table 6**. Inhibitory activity against WT and mutant HIV-1 RT.

| HIV-1 RT | $IC_{50}$ (μM) | | | | |
|---|---|---|---|---|---|
| | **9a** | **K-5a2** | **25a** | **ETR** | **RPV** |
| WT | 0.114±0.029 | 0.076±0.003 | 0.101±0.015 | 0.012±0.002 | 0.015±0.001 |
| L100I | 0.228±0.090 | 0.092±0.027 | 0.099±0.04 | 0.013±0.004 | 0.024±0.012 |
| K103N | 0.222±0.010 | 0.162±0.000 | 0.191±0.022 | 0.025±0.002 | 0.027±0.000 |
| Y181C | 0.141±0.003 | 0.126±0.010 | 0.149±0.005 | 0.017±0.002 | 0.021±0.002 |
| Y188L | 0.452±0.083 | 0.215±0.003 | 0.301±0.071 | 0.046±0.009 | 0.084±0.038 |
| E138K | 0.374±0.203 | 0.200±0.078 | 0.350±0.120 | 0.032±0.011 | 0.041±0.021 |
| V106A/F227L | 0.130±0.013 | 0.222±0.051 | 0.106±0.040 | 0.008±0.002 | 0.015±0.004 |
| K103N/Y181C | 0.120±0.057 | 0.071±0.020 | 0.107±0.052 | 0.019±0.008 | 0.023±0.014 |

Furthermore, **9a**, **K-5a2** and **25a** were tested for their ability to inhibit recombinant WT and a panel of mutant HIV-1 RT enzymes (including L100I, K103N, Y181C, Y188L, E138K, V106A/F227L and K103N/Y181C) with the aim to further evaluate their resistance profile from the perspective of enzyme inhibition activity and validate their binding target. ETR and RPV were selected as control drugs. As depicted in **Table 4**, **9a**, **K-5a2**, and **25a** exhibited similar inhibitory potency against WT RT compared to their activity against RT mutants, respectively, indicating that these compounds indeed harvest a relatively high resistance profile. However, although **9a**, **K-5a2**, and **25a** exhibited more potent activity than ETR and RPV in cell, the RT inhibitory activities of the three compounds were dramatically lower than that of ETR and RPV, and caused about 10-fold change in the $IC_{50}$ values, respectively. We hypothesized that **9a**, **K-5a2**, and **25a** have more hydrogen bond donor and acceptor sites than ETR and RPV[13]. In addition, we noticed that their RT inhibitory activities are quite different from their cellular activity, especially for the selected representative compounds **9a**, **K-5a2**, and **25a.** Actually, the $EC_{50}$ and $IC_{50}$ values are very much depending on the conditions of testing. For the MT-4/MTT method in cell activity testing, the $EC_{50}$ values depends on the number of cells, the quantity of virus (and the ratio of the number of virus particles/number of cells), the replication rounds and the concentration of (serum) proteins in the medium (indicative for protein binding of the compound). For example, the increasing amount virus in the assay could lead to an increase of the $EC_{50}$ value. But, for the RT assay, the $IC_{50}$ values depends on the amounts of template/primer and enzyme[19].

**Molecular modeling studies**

In an attempt to achieve insight into the allosteric binding mode of the most potent compound **9a** with the NNIBP, the molecular modeling studies was performed with the software SurflexeDock SYBYL-X 2.0. Co-crystal structure of WT RT/**25a** (PDB code: 6c0n) and RES056 RT/**25a** (PDB code: 6c0r) were used as the input structures for docking.[15] The docking protocol is the same as our previously report[13]. PyMOL was used to visualize the docking results.

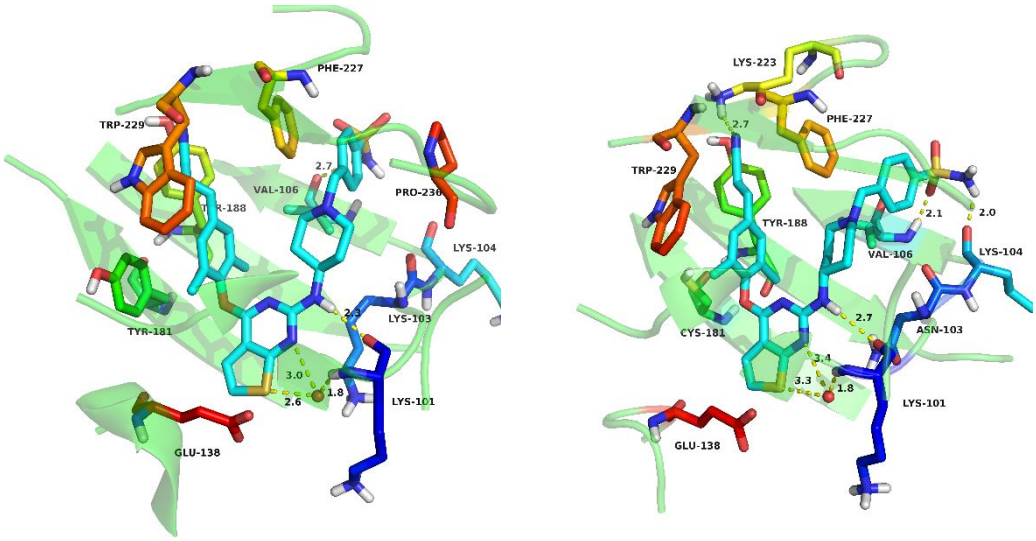


**A** **B**

**Figure 5.** Predicted binding modes of **9a** with WT HIV-1 RT (**A**, PDB code: 6c0n) and RES056 RT (**B**, PDB code: 6c0r). Hydrogen bonds between inhibitors and amino acid residues are indicated with dashed lines (yellow). Nonpolar-hydrogen atoms are not shown for clarity.

As shown in **Figure 5**, **9a** adopt a horseshoe conformation in NNIBP, which is similar to that seen with NNRTIs in the DAPY family[15]. The binding mode of **9a** with HIV-1 WT RT (**Figure 5A**) demonstrated that the left wing structure of **9a** arches into project into the hydrophobic tunnel surrounded by Tyr181, Tyr188, Phe227, and

Trp229, forming π-π interactions with these residues. The amino piperidine-linked sulfonamide structure of the right wing project into the tolerant region I lined by Lys101, Lys103, Lys104, and Val106, developing hydrogen-bonding force with the backbone nitrogen of Lys101 and Val106. Moreover, the S atom and N atom of the newly introduced thiophene[2,3-*d*]pyrimidine scaffold are involved in extensive hydrogen-bonding network with backbone of Lys101 through a bridging water molecule. Examination of the interactions between **9a** and HIV-1 RES056 RT (**Figure 5B**) reveals that all the hydrogen bonds shown in **Figure 5A** are preserved, although there are some variations in the hydrogen bond lengths and π-π interactions. In the binding mode of **9a** with HIV-1 RES056 RT, the Lys103 to Asn103 substitution in RT led to the dramatic changes of the NNIBP and increased the hydrogen bond lengths between the thiophene[2,3-*d*]pyrimidine and Lys101, the Tyr181 to Cys181 substitution result in the greatly reduced π-π stacking interactions between **9a** and Tyr181. However, **9a** are able to establish more stronger hydrogen-bonding with main chain of Lys104 and Val106 by varying the position of the piperidine-linked sulfonamide group to counterbalance the loss of hydrogen bonding, and the Y181C mutation-caused damage could be compensated by its enhanced hydrogen-bonding interactions with Lys223. All these factors accounts for the improved drug resistance profiles of **9a**.

***In Vitro* Effects of 9a on CYP Enzymatic Inhibitory Activity.**

It was reported that ETR is an inhibitor of CYP2C9 and CYP2C19 and an inducer of CYP3A4, which can lead to many drug–drug interactions[20]. Therefore,

inhibition and induction studies with primary CYP isoforms was usually conducted to assess the risk of pharmacokinetic drug interactions before the pharmacokinetic trials. As depicted in **Table 8**, the results revealed that **9a** and **25a** were very weak CYP1A2 inhibitors with $IC_{50}$ values greater than 50 μM. Moreover, both inhibitors exhibited no significant inhibition of CYP2C9, CYP2C19, CYP2D6, and CYP3A4M ($IC_{50}$ > 5 μM) compared to the approved drug RPV ($IC_{50}$ = 0.335-3.41 μM), which preliminarily proved that **9a** and **25a** had no side effect in the liver.

**Table 8.** Effects of **9a** and **25a** on Inhibition of CYP1A2, CYP2C9, CYP2C19, CYP2D6, and CYP3A4M

| Compds | $IC_{50}$ (μM) | | | | |
|---|---|---|---|---|---|
| | CYP1A2 | CYP2C9 | CYP2C19 | CYP2D6 | CYP3A4M |
| **9a** | >50 | 8.37 | 10.5 | 23.8 | 7.95 |
| **25a** | >50 | 13.2 | 21.2 | 15.2 | 5.92 |
| **RPV** | 9.11 | 0.346 | 0.335 | 3.41 | 2.17 |
| **α-Naphthoflavone** | 0.194 | - | - | - | - |
| **Sulfaphenazole** | - | 0.660 | - | - | - |
| **(+)-N-3-benzylnirvanol** | - | - | 0.256 | - | - |
| **Quinidine** | - | - | - | 0.156 | - |
| **Ketoconazole** | - | - | - | - | 0.0366 |

***In Vivo* Pharmacokinetics Study.**

In the pursuit of better RT-binding affinities with RT, multiple lipophilic aromatic rings were introduced to the approved DAPY NNRTIs (ETR and RPV), resulting in their poor aqueous solubility (the solubility of ETR < 1 μg/mL in pH 7.0) and lower bioavailability[21]. Similarly, the lead **25a** also demonstrated low bioavailability ($F$ = 16.19 %) combined with poor aqueous solubility[14]. So, we tested

the solubility of **9a** before the *in vivo* pharmacokinetics study. As shown in **Table 9**, the solubility of **9a** (S = 22.8 μg/mL) at pH 7.0 was much higher than that of **25a** (S = 5.26 μg/mL), ETR (S < 1 μg/mL) and RPV (S < 1 μg/mL). Moreover, it also exhibited excellent solubility at pH 2.0 (S = 78.6 μg/mL). Encouraged by its improved solubility, the pharmacokinetics study was further conducted in Wistar rat pharmacokinetics (PK) model (**Table 10** and **Figure 6**). After a single 2 mg/kg *iv* dose, **9a** was characterized by a modest clearance (CL = 2.3 L/h/kg) and half-life ($T_{1/2}$ = 2.0 h). Absorption of **9a** was evaluated after being dosed at 20 mg/kg, the plasma concentration reached maximum ($T_{max}$) at 3.2 h with $C_{max}$ value of 614 ng/mL, and the $t_{1/2}$ of **9a** was 2.8 h. Notably, the oral bioavailability (*F*) was 37.06 %, that is about 2.3-fold higher than that of **25a** and sufficiently higher enough for a potential drug candidate.

**Table 9**. The Aqueous Solubility of **9a**

| Compds | aqueous solubility (μg/mL)[a] | | |
|---|---|---|---|
| | pH 7.4 | pH 7.0 | pH 2.0 |
| **9a** | <1 | 22.8 | 78.6 |
| **25a** | <1 | 5.26 | 84.7 |
| **ETR** | <1 | <1 | 127 |
| **RPV** | <1 | <1 | 103 |

[a] Measured with HPLC method.

**Table 10**. Pharmacokinetic Profile of **9a**[a]

| Subject | $T_{1/2}$ (h) | $T_{max}$ (h) | $C_{max}$ (ng/mL) | $AUC_{0-t}$ (h*ng/mL) | $AUC_{0-\infty}$ (h*ng/mL) | CL (L/h/kg) | F (%) |
|---|---|---|---|---|---|---|---|
| **9a** (iv)[b] | 2.0±0.4 | 0.033 | 1713±399 | 814±179 | 887±174 | 2.3±0.4 | - |
| **9a** (po)[c] | 2.8±0.3 | 3.2±0.9 | 614±249 | 3017±547 | 3287±517 | - | 37.06 |

[a] PK parameter (mean ± SD, n = 5), [b] Dosed intravenously at 2 mg/kg, [c] Dosed orally at 20 mg/kg.

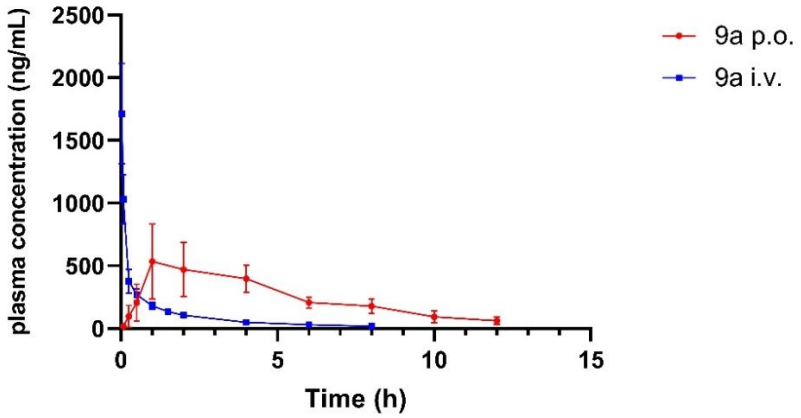


**Figure 6**. The plasma concentration–time profiles of **9a** in rats following oral administration (20 mg.kg$^{-1}$) and intravenous administration (2 mg.kg$^{-1}$).

## Safety Assessment

### Assessment of Acute Toxicity.

The favorable PK profile of **9a** along with its improved drug resistance profiles against HIV-1 mutant strains warranted its use in *in vitro* safety studies. The maximum tolerated dose of **9a** was further determined for acute toxicity in Kunming mice. The lead compounds **25a** and RPV were selected as the references. A total of 40 mice were randomly divided into four groups and given single oral doses of 0 mg/kg (control group), 2000 mg/kg of **9a**, **25a** and RPV on the first day, respectively (**Figure 7**). The mice did not exhibit any toxic symptoms or mortality immediately during the post-treatment period of 14 days. No abnormal behaviors or significant changes of the body weight were observed during the period of the experiments. The results demonstrated that **9a** was well-tolerated up to a dose of 2000 mg/kg with no acute toxicity.

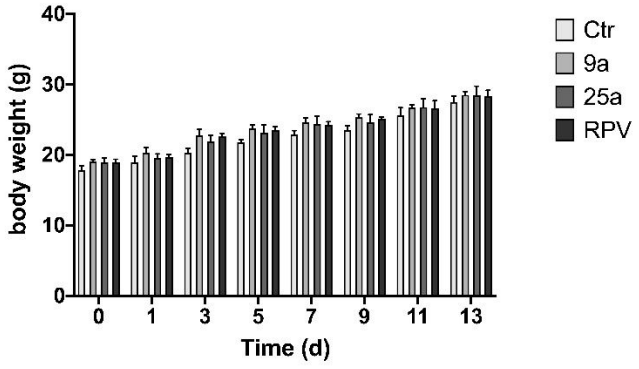


**Figure 7**. The relative body weight changes of mice in different groups.

## Assessment of hERG activity

The inhibition of the hERG channel by noncardiovascular drugs is a side effect that severely impedes the development of novel medications, and it is becoming more important to screen the compounds activity against the hERG potassium channel in order to estimate the potential risk for cardiotoxicity[22]. Thus, the promising compound **9a** was further evaluated for its activity in the hERG ion channel with manual patch-clamp electrophysiology approach. As shown in **Figure 8**, **9a** exhibited much reduced QT liability and lower hERG inhibition ($IC_{50}$ = 0.979 μM) in comparison with that of the lead **25a** ($IC_{50}$ = 0.186 μM), **K-5a2** ($IC_{50}$ = 0.130 μM) and the approved NNRTIs drug RPV ($IC_{50}$ = 0.50 μM)[21].

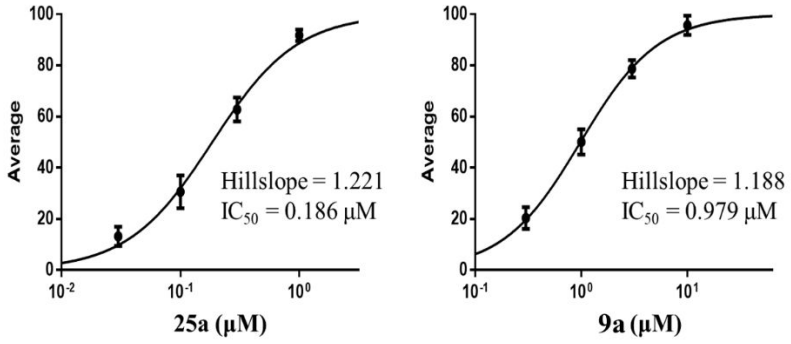


**Figure 8.** Activity of **9a** against hERG potassium channel in HEK293 cells.

## Conclusion

Although second-generation NNRTIs achieved success in suppressing HIV-1 replication and reducing viral loads, the rapid development of drug-resistant mutations in HIV-1 RT, dose-limiting toxicity, and the poor pharmacokinetic properties remains a major impediment to effective anti-HIV therapy. Our previous efforts using structural mimics of a range of scaffolds or peripheral substituents have produced a series of piperidine-substituted thiophene[2,3-*d*]pyrimidine based NNRTIs that have single-nanomolar level antiviral potency in HIV-infected MT-4 cells. However, the most promising inhibitors **K-5a2** and **25a** also ran into the similar problems. In the current study, a series of novel piperidine-substituted thiophene[2,3-*d*]pyrimidine derivatives were designed and synthesized. Compound **9a** proved to be an exceptionally potent inhibitor in MT-4 cells, yielding significantly more potent anti-HIV-1 activity than ETR against all of the tested WT and NNRTI-resistant HIV-1 strain, with $EC_{50}$ values of 3.24 nM (WT), 2.05 nM (L100I), 2.34 nM (K103N), 6.57 nM (Y181C), 7.59 nM (Y188L), 6.70 nM (E138K), 4.81 nM (F227L+V106A), and 6.45 nM (RES056). RT inhibitory activity results further demonstrated that **9a** has a relatively high resistance profile. Moreover, HIV-1 ($III_B$) was passaged for 30 generations in cell culture in the presence of increasing concentrations of **9a**, **25a** and **K-5a2** to explore further insight into understanding their antiviral resistance. The RT-encoding regions of the HIV-1($III_B$) strains selected in the presence of **9a** was sequenced. Several mutations were detected in comparison with the DNA sequence of the WT HIV-1($III_B$) strain, including K101E, V108I,

F227C and M230I. Then the antiviral activity of **9a** against the selected strains in MT-4 cells was determined to confirm the drug resistance. Indeed, **9a** exhibited 888-fold reduced susceptibility. Encouragingly, the activity of NRTIs drug AZT against $9a^{res}$ strain ($EC_{50}$ = 0.0010 μM) was about 12 times potent than against HIV-1 $III_B$ ($EC_{50}$ = 0.0127 μM). The distinct antiviral resistance profiles of our NNRTIs **9a** support its potential in the future anti-HIV HAART therapy.

Furthermore, the solubility of **9a** in water (pH = 7.0) is greatly increased (S = 22.8 μg/mL). **9a** has weaker inhibitory effect to primary CYP isoforms ($IC_{50}$ > 5.0 μM) and hERG channel ($IC_{50}$ = 0.979 μM), suggesting its negligible drug-drug interactions and lower risk for cardiotoxicity, compared to the lead **25a**. Moreover, **9a** exhibited *in vivo* favorable pharmacokinetic properties in rats ($F$ = 37.06 %) and safety in mice ($LD_{50}$ > 2000 mg/kg). The promising *in vitro* and *in vivo* results highlights that compound **9a** has enormous potential as a next generation anti-HIV-1 drug candidate.

## EXPERIMENTAL SECTION

### Chemistry

All melting points were determined on a micro melting point apparatus (RY-1G, Tianjin Tian Guang Optical Instruments). $^1$H-NMR and $^{13}$C-NMR spectra were recorded in DMSO-$d_6$ on a Bruker AV-400 spectrometer with tetramethylsilane (TMS) as the internal standard. Chemical shifts are reported in $\delta$ values (ppm) from TMS and coupling constants are given in hertz; signals are abbreviated as s (singlet), d (doublet), t (triplet), and m (multiplet). The mass spectra were measured in A

G1313A Standard LC Autosampler (Agilent). All reactions were routinely monitored by thin layer chromatography (TLC) on Silica Gel GF254 for TLC (Merck), and spots were visualized with iodine vapor or by irradiation with UV light (λ = 254). Flash column chromatography was performed on columns packed with Silica Gel (200-300 mesh, Qingdao Haiyang Chemical Company). Solvents were purified and dried by standard methods. Compounds purity was analyzed on a Shimadzu SPD-20A/20AV HPLC system with a Inertsil ODS-SP, 5 μm $C_{18}$ column (150 mm × 4.6 mm). HPLC conditions: methanol/water 75:25; flow rate 1.0 mL/min; UV detection from 210 to 400 nm; temperature, ambient; injection volume, 10 μL. Purity of all final compounds was >95%.

**4-((2-chlorothieno[2,3-*d*]pyrimidin-4-yl)oxy)-3,5-dimethylbenzaldehyde (6)**

A mixture of 4-hydroxy-3,5-dimethylbenzaldehyde (1.76 g, 11.7 mmol) and $K_2CO_3$ (2.70 g, 19.5 mmol) in 40 mL of DMF was stirred at room temperature for 15 min, and then 2,4-dichlorothiopheno[2,3-*d*]pyrimidine (**5**, 2.0 g, 9.76 mmol) was added to the mixture. The mixture was stirred for another 1.5 h and then poured into ice water (200 mL) and left to stand for 20 min. The obtained precipitated was filtrated and washed with cold water, recrystallized from DMF-$H_2O$ to provide intermediate **6** as a white solid in 85% yield, mp: 263-265°C. ESI-MS: m/z 319.4 (M + 1), 341.2 (M + Na). $C_{15}H_{11}ClN_2O_2S$ (318.02).

**(*E*)-3-(4-((2-chlorothieno[2,3-*d*]pyrimidin-4-yl)oxy)-3,5-dimethylphenyl) acrylonitrile (7)**

A mixture of $(EtO)_2P(O)CH_2CN$ (1.34 g, 7.52 mmol) and *t*-BuOK (1.42 g, 12.5

mmol) in THF (25 mL) was stirred for 1 h at 0 °C, and then a solution of **6** (2.0 g, 6.28 mmol) in THF (15 mL) and DCM (15 mL) was slowly added over 1 h. The mixture was stirred for another 4 hours at room temperature and then poured into ice water (60 mL). The precipitate was collected and washed with water to give intermediate **7** as a white solid in 72% yield, mp: 235-237°C. ESI-MS: m/z 342.4 (M + 1), 364.2 (M + Na). $C_{17}H_{12}ClN_3OS$ (341.04).

**(*E*)-3-(3,5-dimethyl-4-((2-(piperidin-4-ylamino)thieno[2,3-*d*]pyrimidin-4-yl)oxy)phenyl)acrylonitrile (8)**

Compound **7** (0.34 g, 1.0 mmol), *N*-Boc-4-aminopiperidine (0.24 g, 1.2 mmol), and anhydrous $K_2CO_3$ (0.28 g, 2 mmol) were added in DMF (10 mL) and refluxing 8 h under magnetic stirring (monitored by TLC). Then the mixed solution was cooled to room temperature and 50 mL of ice water was added. The resulting precipitate was collected and dissolved in DCM (5 mL) and trifluoroacetic acid (TFA) (0.74 mL, 10 mmol). The mixed solution was stirred for another 3 h (monitored by TLC) at room temperature. Then the reaction solution was alkalized to pH 9 with saturated sodium bicarbonate solution and washed with saturated sodium chloride solution (10 mL). The aqueous phase was extracted with DCM (3 × 5 mL). Then the combined organic phase was dried over anhydrous $Na_2SO_4$, filtered, and concentrated under reduced pressure to give **8** as a white solid in 71% yield, mp 123−125°C. ESI-MS: m/z 406.3 (M + 1). $C_{22}H_{23}N_5OS$ (405.16).

**General procedure for the preparation of final compounds 9a-e**

Compound **8** (0.40 g, 1.0 mmol) and anhydrous $K_2CO_3$ (0.17 g, 1.2 mmol) were

added to anhydrous DMF (10 mL), which was followed by addition of appropriate substituted benzyl chloride (bromine) (1.1 equiv). The reaction mixture was stirred at room temperature for 4-8 h (monitored by TLC). Then the solvent was removed under reduced pressure, and water (30 mL) was added, extracted with ethyl acetate (3 × 15 mL), and the organic phase was washed with saturated sodium chloride (10 mL), then dried over anhydrous $Na_2SO_4$ to give the corresponding crude product, which was purified by flash column chromatography and recrystallized from ethyl acetate (EA)/petroleum ether (PE) to afford the target compounds **9a-e**.

**(*E*)-4-((4-((4-(4-(2-cyanovinyl)-2,6-dimethylphenoxy)thieno[2,3-*d*]pyrimidin-2-yl) amino)piperidin-1-yl)methyl)benzenesulfonamide (9a).**

Recrystallized from EA/PE as a white solid, 67% yield, mp: 205-207°C. $^1$H NMR (400 MHz, DMSO-$d_6$) δ 7.78 (d, $J$ = 8.2 Hz, 2H, $C_3$,$C_5$-Ph'-H), 7.61 (d, $J$ = 13.6 Hz, 1H, ArCH ═ ), 7.48-7.45 (m, 4H), 7.35 (d, $J$ = 5.9 Hz, 1H, $C_7$-thienopyrimidine-H), 7.31 (s, 2H, $SO_2NH_2$), 7.25 (d, $J$ = 6.0 Hz, 1H, $C_6$-thienopyrimidine-H), 7.07 (s, 1H, NH), 6.43 (d, $J$ = 16.7 Hz, 1H, ═CHCN), 3.72-3.70 (m, 1H), 3.49 (s, 2H, N-$CH_2$), 2.74-2.72 (m, 2H), 2.08 (s, 6H), 1.99-1.27 (m, 6H). $^{13}$C NMR (100 MHz, DMSO-$d_6$) δ 162.6, 159.3, 150.5, 143.4, 143.1, 131.7, 131.7, 129.4, 128.6, 126.0, 119.4, 118.9, 96.7, 62.0, 60.2, 52.7, 31.6, 21.1, 16.6, 14.5. ESI-MS: m/z 575.3 $[M + 1]^+$, 597.5 $[M + Na]^+$. $C_{29}H_{30}N_6O_3S_2$ (574.18). HPLC purity: 99.37%.

**(*E*)-4-((4-((4-(4-(2-cyanovinyl)-2,6-dimethylphenoxy)thieno[2,3-*d*]pyrimidin-2-yl) amino)piperidin-1-yl)methyl)benzamide (9b)**

Recrystallized from EA/PE as a white solid, 72% yield, mp: 221-223°C. $^1$H NMR (400 MHz, DMSO-$d_6$) δ 7.80 (d, $J$ = 8.0 Hz, 2H, $C_3$,$C_5$-Ph'-H), 7.62 (d, $J$ = 16.6 Hz, 1H, ArCH ＝), 7.72 (s, 2H, $C_3$,$C_5$-Ph''-H), 7.54 (d, $J$ = 8.1 Hz, 2H, $C_2$,$C_6$-Ph'-H), 7.34 (d, $J$ = 5.6 Hz, 1H, $C_7$-thienopyrimidine-H), 7.22 (d, $J$ = 6.0 Hz, 1H, $C_6$-thienopyrimidine-H), 7.01 (s, 1H, NH), 6.41 (d, $J$ = 16.7 Hz, 1H, ＝CHCN), 3.73-3.70 (m, 1H), 3.49 (s, 2H, N-$CH_2$), 2.73-2.72 (m, 2H), 2.08 (s, 6H), 1.89-1.21 (m, 6H). $^{13}$C NMR (100 MHz, DMSO-$d_6$) δ 164.8, 162.8, 143.5, 143.0, 131.4, 129.4, 128.5, 126.1, 124.0, 118.7, 105.3, 61.8, 60.0, 52.7, 31.6, 21.2, 16.8, 14.3. ESI-MS: m/z 539.2 $[M + 1]^+$, 561.3 $[M + Na]^+$. $C_{30}H_{30}N_6O_2S$ (538.21). HPLC purity: 98.94%.

**(*E*)-3-((4-((4-(4-(2-cyanovinyl)-2,6-dimethylphenoxy)thieno[2,3-*d*]pyrimidin-2-yl) amino)piperidin-1-yl)methyl)benzamide (9c)**

Recrystallized from EA/PE as a white solid, 66% yield, mp: 217-219°C. $^1$H NMR (400 MHz, DMSO-$d_6$) δ 7.90-7.86 (m, 3H), 7.72 (s, 2H, $C_3$,$C_5$-Ph''-H), 7.62 (d, $J$ = 16.7 Hz, 1H, ArCH ＝), 7.56-7.53 (m, 1H), 7.34 (d, $J$ = 5.5 Hz, 1H, $C_7$-thienopyrimidine-H), 7.23 (d, $J$ = 5.6 Hz, 1H, $C_6$-thienopyrimidine-H), 7.01 (s, 1H, NH), 6.42 (d, $J$ = 16.5 Hz, 1H, ＝CHCN), 3.72 (s, 1H), 3.49 (s, 2H, N-$CH_2$), 2.76-2.75 (m, 2H), 2.08 (s, 6H), 1.89-1.23 (m, 6H). $^{13}$C NMR (100 MHz, DMSO-$d_6$) δ 168.2, 164.8, 159.3, 144.8, 142.3, 137.5, 133.4, 133.0, 131.3, 128.9, 128.9, 127.8, 123.9, 118.8, 52.7, 50.6, 31.6, 29.0, 16.6, 14.3. ESI-MS: m/z 539.3 $[M + 1]^+$, 561.7 $[M + Na]^+$. $C_{30}H_{30}N_6O_2S$ (538.21). HPLC purity: 97.43%.

**ethyl (*E*)-4-((4-((4-(4-(2-cyanovinyl)-2,6-dimethylphenoxy)thieno[2,3-*d*]pyrimidin -2-yl)amino)piperidin-1-yl)methyl)benzoate (9d)**

Recrystallized from EA/PE as a white solid, 59% yield, mp: 207-209°C. $^1$H NMR (400 MHz, DMSO-$d_6$): $\delta$ 7.86 (d, $J$ = 8.2 Hz, 2H, $C_3$,$C_5$-Ph'-H), 7.72 (s, 2H, $C_3$,$C_5$-Ph''-H), 7.62 (d, $J$ = 16.6 Hz, 1H, ArCH ＝),7.34 (d, $J$ = 5.7 Hz, 1H, $C_7$-thienopyrimidine-H), 7.23 (d, $J$ = 5.6 Hz, 1H, $C_6$-thienopyrimidine-H), 7.13 (d, $J$ = 8.2 Hz, 2H, $C_2$,$C_6$-Ph'-H), 7.02 (s, 1H, NH), 6.42 (d, $J$ = 16.6 Hz, 1H, ＝CHCN), 4.32 (q, $J$ = 7.2 Hz, 2H, $CO_2CH_2$), 3.73-3.72 (m, 1H), 3.49 (s, 2H, N-$CH_2$), 2.74 (s, 2H), 2.09 (s, 6H), 1.96-1.37 (m, 6H), 1.32 (t, $J$ = 7.1 Hz, 3H, $CH_2C\underline{H}_3$). $^{13}$C NMR (100 MHz, DMSO-$d_6$): $\delta$ 162.5, 160.7, 143.5, 142.9, 131.8, 129.5, 127.5, 127.0, 125.3, 123.5, 120.4, 118.7, 109.7, 60.8, 60.0, 52.6, 31.4, 21.3, 16.6 14.6, 14.2. ESI-MS: m/z 568.3 $[M + 1]^+$, 590.1 $[M + Na]^+$. $C_{32}H_{33}N_5O_3S$ (567.23). HPLC purity: 99.02%.

**(*E*)-3-(4-((2-((1-(4-fluorobenzyl)piperidin-4-yl)amino)thieno[2,3-*d*]pyrimidin-4-yl)oxy)-3,5-dimethylphenyl)acrylonitrile (9e)**

Recrystallized from EA/PE as a white solid, 78% yield, mp: 224-226°C. $^1$H NMR (400 MHz, DMSO-$d_6$) δ 7.82 (d, $J$ = 8.2 Hz, 2H, $C_3$,$C_5$-Ph'-H), 7.62 (d, $J$ = 16.6 Hz, 1H, ArCH ＝), 7.72 (s, 2H, $C_3$,$C_5$-Ph''-H), 7.53 (d, $J$ = 8.1 Hz, 2H, $C_2$,$C_6$-Ph'-H), 7.34 (d, $J$ = 5.9 Hz, 1H, $C_7$-thienopyrimidine-H), 7.23 (d, $J$ = 5.6 Hz, 1H, $C_6$-thienopyrimidine-H), 7.01 (s, 1H, NH), 6.42 (d, $J$ = 16.6 Hz, 1H, ＝CHCN), 3.72 (s, 1H), 3.49 (s, 2H, N-$CH_2$), 2.74-2.72 (m, 2H), 2.08 (s, 6H), 1.92-1.34 (m, 6H). $^{13}$C NMR (100 MHz, DMSO-$d_6$) δ 164.8, 162.8, 160.3, 143.5, 143.1, 131.4, 129.7, 128.5, 126.1, 125.2, 124.0, 118.7, 105.3, 96.7, 61.8, 60.0, 52.7, 31.6, 21.3, 16.8, 14.4. ESI-MS: m/z 521.3 $[M + 1]^+$, 543.2 $[M + Na]^+$. $C_{30}H_{28}N_6OS$ (520.20). HPLC purity: 97.32%.

**(*E*)-4-((4-((4-(4-(2-cyanovinyl)-2,6-dimethylphenoxy)thieno[2,3-*d*]pyrimidin-2-yl) amino)piperidin-1-yl)methyl)benzonitrile (9f)**

Recrystallized from EA/PE as a white solid, 67% yield, mp: 231-233°C. $^{1}$H NMR (400 MHz, DMSO-$d_6$) δ 7.80 (d, $J$ = 8.1 Hz, 2H, $C_3$,$C_5$-Ph'-H), 7.62 (d, $J$ = 16.7 Hz, 1H, ArCH ═ ), 7.73 (s, 2H, $C_3$,$C_5$-Ph''-H), 7.51 (d, $J$ = 8.0 Hz, 2H, $C_2$,$C_6$-Ph'-H), 7.34 (d, $J$ = 6.1 Hz, 1H, $C_7$-thienopyrimidine-H), 7.22 (d, $J$ = 6.3 Hz, 1H, $C_6$-thienopyrimidine-H), 7.01 (s, 1H, NH), 6.41 (d, $J$ = 16.6 Hz, 1H, ═CHCN), 3.71 (s, 1H), 3.49 (s, 2H, N-$CH_2$), 2.73-2.70 (m, 2H), 2.08 (s, 6H), 1.94-1.36 (m, 6H). $^{13}$C NMR (100 MHz, DMSO-$d_6$) δ 164.8, 162.8, 145.2, 143.0, 131.4, 129.7, 128.5, 126.1, 125.1, 124.0, 118.8, 105.3, 96.7, 61.8, 52.7, 48.5, 31.6, 21.2, 16.8, 14.4. ESI-MS: m/z 514.2 $[M + 1]^+$, 536.5 $[M + Na]^+$. $C_{29}H_{28}FN_5OS$ (513.19). HPLC purity: 96.92%.

**Materials and methods**

***In vitro anti-HIV assay***

The anti-HIV activity tests were performed in MT-4 cells using the MTT method[23]. Stock solutions (10 x final concentration) of the test compounds were added in 25 μL volumes to two series of triplicate wells so as to allow simultaneous evaluation of their effects on mock- and HIV-infected cells at the beginning of each experiment. Serial 5-fold dilutions of test compounds were made directly in flat-bottomed 96-well microtiter trays using a Biomek 3000 robot (Beckman instruments, Fullerton, CA). Untreated HIV- and mock-infected cell samples were included as controls. HIV stock (50 μL) at 100-300 $CCID_{50}$ (50 % cell culture

infectious doses) or culture medium was added to either the infected or mock-infected cell wells of the microtiter tray. Mock-infected cells were used to evaluate the effects of test compound on uninfected cells in order to assess the cytotoxicity of the test compounds. Exponentially growing MT-4 cells were centrifuged for 5 minutes at 220 g and the supernatant was discarded. The MT-4 cells were resuspended at 6 x $10^5$ cells/mL and 50 µL volumes were transferred to the microtiter tray wells. Five days after infection, the viability of mock-and HIV-infected cells was examined spectrophotometrically using the MTT assay. The MTT assay is based on the reduction of yellow colored 3-(4,5-dimethylthiazol-2-yl)-2,5-diphenyltetrazolium bromide (MTT) (Acros Organics) by mitochondrial dehydrogenase activity in metabolically active cells to a blue-purple formazan that can be measured spectrophotometrically. The absorbances were read in an eight-channel computer-controlled photometer (Infinite M1000, Tecan), at two wavelengths (540 nm and 690 nm). All data were calculated using the median absorbance value of three wells. The 50% cytotoxic concentration ($CC_{50}$) was defined as the concentration of the test compound that reduced the absorbance ($OD_{540}$) of the mock-infected control sample by 50%. The concentration achieving 50% protection against the cytopathic effect of the virus in infected cells was defined as the 50% effective concentration ($EC_{50}$).

***In vitro selection of HIV-1 ($III_B$) mutant strains***

HIV-1 strains resistant to **9a**, **25a**, and **k-5a2** were obtained after sequential passaging of HIV-1 $III_B$ in the presence of increasing concentrations of **9a**, **25a**, and

**k-5a2,** respectively, in MT-4 cells[24]. At the start of the selection, MT-4 cells were inoculated with HIV-1 $III_B$ virus strain in the presence of a 3.5 nM of **9a**, 1.2 nM concentration of **25a**, and 1.5 nM of **k-5a2,** respectively. The cultures were passaged every 3-4 days. When cytopathogenic effect (CPE) was observed, cell culture supernatant was used as inoculum to infect new MT-4 cells at the same concentration of compound. The second time CPE was observed the concentration of compound was increased. After serial passaging (30 passages) we were able to culture resistant virus in the presence of 260 nM, 275 nM and 870 nM of **9a**, **25a**, and **k-5a2**, respectively. In a parallel control experiment, HIV-1 ($III_B$) was cultured in MT-4 cells in the absence of any compound.

***Genotypic evaluation***

RNA was extracted from virus stock using the QIAamp Viral RNA mini Kit (QIAgen, Venlo, The Netherlands) as described in the Manufacturer's protocol. The procedures for the preparation of samples for RT-PCR, amplification and sequencing have been reported elsewhere[25, 26].

***HIV-1 RT inhibition assay***

The HIV-RT inhibition assay was performed by using the ELISA method[27]. Briefly, the reaction mixture containing HIV-1 RT enzyme, reconstituted template and viral nucleotides [digoxigenin (DIG)-dUTP, biotin-dUTP and dTTP] in the incubation buffer with or without inhibitors was incubated for 1 h at 37ºC. Then, the reaction mixture was transferred to a streptavidin-coated microtitre plate (MTP) and incubated for another 1 h at 37ºC. The biotin-labeled dNTPs that were incorporated

into the cDNA chain in the presence of RT were bound to streptavidin. The unbound dNTPs were washed with washing buffer, and anti-DIG-POD was added to the MTPs. After incubation for 1 h at 37ºC, the DIG-labeled dNTPs incorporated in cDNA were bound to the anti-DIG-POD antibody. The unbound anti-DIG-PODs were washed out and the peroxide substrate (ABST) solution was added to the MTPs. The absorbance of the sample was determined at OD405 nm using a microtiter plate ELISA reader. The percentage inhibitory activity of RT inhibitors was calculated according to the following formula: % Inhibition = [O.D. value with RT but without inhibitors - O.D. value with RT and inhibitors]/[O.D. value with RT and inhibitors - O.D. value without RT and inhibitors]. The $IC_{50}$ values correspond to the concentrations of the inhibitors required to inhibit biotin-dUTP incorporation by 50%.

***Cytochrome P450 inhibition assay***

Compound **9a** at eight concentrations (0, 0.05, 0.15, 0.5, 1.5, 5.0, 15, 50 μM) was incubated with human liver microsomes (0.25 mg/mL) and NADPH (10 mM) in the presence of CYP1A2 probe substrate phenacetin (100 μM), CYP2C9 probe substrate diclofenac (50 μM), CYP2C19 probe substrate S-mephenytoin (300 μM), CYP2D6 probe substrate dextromethorphan (50 μM), and CYP3A4M probe substrate midazolam (20 μM) for 10 min in a 37°C water bath. Then, the selective CYP1A2 inhibitor alpha-naphthoflavone, the selective CYP2C9 inhibitor sulfaphenazole, the selective CYP2C19 inhibitor (+)-*N*-3-benzylnirvanol, the selective CYP2D6 inhibitor quinidine, the selective CYP3A4M inhibitor ketoconazole was screened alongside the test compound as a positive control (concentration: 0, 0.0142, 0.0123, 0.037, 0.11,

0.33, 1.0, 3.0 μM), respectively. Methanol containing tolbutamide as internal standard was used for stopping the reaction. Positive controls, duplicates of **9a** for each concentration were prepared in parallel.

***Assay procedures for hERG activity***

The inhibitory activity against the hERG potassium channel was tested in HEK293 cells which were stably transfected with hERG cDNA[28]. HEK239 cells expressing hERG were cultured in 35 mm dishes for 24 hours and kept at 37°C under 5% $CO_2$. A micropipette was drawn out from borosilicate glass to give a tip resistance between 3 ~ 5 MΩ. For each trial, one dish of cells was removed from the incubator, washed twice and placed on the microscope. The whole-cell recordings were performed using a commercial patch clamp amplifier.

Tail currents were evoked once every 30 s by a 3 s, -50 mV repolarizing pulse following a 2 s, +50 mV depolarizing pulse with a stable voltage of -80 mV. The voltage protocol started with a 50ms depolarization pulse of -50mv, which served as the baseline for calculating the peak tail current amplitude. Only stable cells with recording parameters exceeding the threshold were used in the experiments. The hERG current was allowed to stabilize for 3 minutes. The cells were kept in the test solution until the peak tail current was stable (< 5% change) for ~5 sweeps. Peak tail amplitudes were then plotted as a function of the sweep number. Before testing the composite application, the average of the five peak tail currents in the steady state was taken as the control current amplitude. Four or five peak tail current measurements at the steady state after test compound application were averaged as the residual current

amplitude after the test compound was suppressed.

***Pharmacokinetics assays***

Ten male Wistar rats (180-200 g) were randomly divided into two groups to receive intravenous (2 $mg.kg^{-1}$) and oral administration (20 $mg.kg^{-1}$) of the compounds. A solution of **9a** was prepared by dissolving in polyethylene glycol (peg) 400/normal saline (65/35, V/V). Blood samples of the intravenous group were collected from the jugular sinus at 2 min, 5 min, 15 min, 30 min, 1 h, 1.5 h, 2 h, 4 h, and 8 h after dosing, and blood samples of the oral administration group were collected at 5 min, 15 min, 30 min, 1 h, 2 h, 4 h, 6 h, 8h, 10 h, and 12 h after dosing (200 μL of blood each times). All the samples were then centrifuged at 8000 rpm for 8 min to separate plasma. The concentration of **9a** in plasma was determined by LC-MS/MS analysis. Briefly, 50 μL of plasma was added to 50 μL of internal standard and 300 μL of methanol in a 5 mL centrifugation tube, which was centrifuged at 3000g for 10 min. The supernatant layer was collected and a 20 μL aliquot was injected for LC-MS/MS analysis. Standard curves for **9a** in blood were generated by the addition of various concentrations of **9a** together with internal standard to blank plasma. Then all samples were quantified with an Agilent 1200 LC/MSD (Agilent, USA). The mobile phase was methanol/1.5% glacial acetic acid (60:40, V/V) at a flow rate of 1.0 mL/min.

***Acute toxicity experiment***

The acute toxicity experiment was carried out in Kunming mice (18-20 g), which were purchased from the animal experimental center of Shandong University.

Compounds were suspended in PEG-400 and normal saline at concentrations of 100 mg•mL$^{-1}$, and administered intragastrical by gavage after the mice had been fasted for 12 hours. A dose of 2000 mg•kg$^{-1}$ was administered to 10 mice per group (5 males, 5 females). Mice were observed for any abnormal behavior and mortality, and weighed 2 h after administered and then every 48 h for 14 days.

## ASSOCIATED CONTENT

The Supporting Information is available free of charge on the ACS Publications website at DOI:

Molecular formula strings and some data (CSV)

## AUTHOR INFORMATION

### Corresponding Authors

*C.P.: e-mail, christophe.pannecouque@rega.kuleuven.be.; tel, 32-(0)16-332171;

*X.L.: e-mail, xinyongl@sdu.edu.cn; tel, 086-531-88380270.

*P.Z.: e-mail, zhanpeng1982@sdu.edu.cn; tel, 086-531-88382005;

### Notes

The authors declare that all experimental work complied with the institutional guidelines on animal studies (care and use of laboratory animals).

The authors declare no competing financial interest.

## ACKNOWLEDGMENTS

We gratefully acknowledge financial support from the National Natural Science Foundation of China (NSFC Nos. 81973181, 81903453), the Key Project of NSFC for International Cooperation (No. 81420108027), Shandong Provincial Natural Science

Foundation (ZR2019BH011), China Postdoctoral Science Foundation (2019T120596), Young Scholars Program of Shandong University (YSPSDU No. 2016WLJH32), Shandong Provincial Key research and development project (Nos. 2017CXGC1401, 2019JZZY021011), the Taishan Scholar Program at Shandong Province. The technical assistance of Mr. Kris Uyttersprot and Mrs. Kristien Erven, for the HIV experiments is gratefully acknowledged.

## ABBREVIATIONS USED

AZT, zidovudine; AIDS, acquired immune deficiency syndrome; $CC_{50}$, 50% cytotoxicity concentration; $C_{max}$, maximum concentration; CYP, cytochrome P450 proteins; DAPY, diarylpyrimidine; DLV, delavirdine; DOR, doravirine; EFV, efavirenz; ETR, etravirine; $EC_{50}$, the effective concentration causing 50% inhibition of viral cytopathogenicity; HAART, highly active antiretroviral therapy; HIV, human immunodeficiency virus; hERG, the human ether-à-go-go related gene; NNIBP, NNRTI-binding pocket; NNRTI, non-nucleoside reverse transcriptase inhibitor; NRTI, nucleoside reverse transcriptase inhibitor; NVP, nevirapine; PMPA, tenofovir; PK, pharmacokinetics; RF, fold-resistance; RPV, rilpivirine; RT, reverse transcriptase; SI, selectivity index; WT, wild-type.

## REFERENCES

1. Namasivayam, V.; Vanangamudi, M.; Kramer, V. G.; Kurup, S.; Zhan, P.; Liu, X.; Kongsted, J.; Byrareddy, S. N. The journey of HIV-1 non-nucleoside reverse transcriptase inhibitors (NNRTIs) from lab to clinic. *J. Med. Chem.* **2019,** 62, 4851-4883.

2. Zhan, P.; Pannecouque, C.; De, C. E.; Liu, X. Anti-HIV drug discovery and development: current innovations and future trends. *J. Med. Chem.* **2016,** 59, 2849-2878.

3. Bec, G.; Meyer, B.; Gerard, M. A.; Steger, J.; Fauster, K.; Wolff, P.; Burnouf, D.; Micura, R.; Dumas, P.; Ennifar, E. Thermodynamics of HIV-1 reverse transcriptase in action elucidates the mechanism of action of non-nucleoside inhibitors. *J. Am. Chem. Soc.* **2013,** 135, 9743-9752.

4. Kang, D.; Feng, D.; Ginex, T.; Zou, J.; Wei, F.; Zhao, T.; Huang, B.; Sun, Y.; Desta, S.; De Clercq, E.; Pannecouque, C.; Zhan, P.; Liu, X. Exploring the hydrophobic channel of NNIBP leads to the discovery of novel piperidine-substituted thiophene[3,2-*d*]pyrimidine derivatives as potent HIV-1 NNRTIs. *Acta Pharm. Sinica B* **2019**, https://doi.org/10.1016/j.apsb.2019.08.013.

5. Kang, D.; Zhao, T.; Wang, Z.; Feng, D.; Zhang, H.; Huang, B.; Wu, G.; Wei, F.; Zhou, Z.; Jing, L.; Zuo, X.; Tian, Y.; Poongavanam, V.; Kongsted, J.; De Clercq, E.; Pannecouque, C.; Zhan, P.; Liu, X. Discovery of piperidine-substituted thiazolo[5,4-*d*]pyrimidine derivatives as potent and orally bioavailable HIV-1 non-nucleoside reverse transcriptase inhibitors. *Commu. Chem.* **2019,** 2, 74.

6. Huang, B.; Chen, W.; Zhao, T.; Li, Z.; Jiang, X.; Ginex, T.; Vilchez, D.; Luque, F. J.; Kang, D.; Gao, P.; Zhang, j.; Tian, Y.; Daelemans, D.; De, C. E.; Pannecouque, C.; Zhan, P.; Liu, X. Exploiting the tolerant region I of the non-nucleoside reverse transcriptase inhibitor (NNRTI) binding pocket: discovery of potent diarylpyrimidine-typed HIV-1 NNRTIs against wild-type and E138K mutant virus with significantly improved water solubility and favorable safety profiles. *J. Med. Chem.* **2019,** 62, 2083-2098.

7. Kang, D.; Zhang, H.; Wang, Z.; Zhao, T.; Ginex, T.; Luque, F. J.; Yang, Y.; Wu, G.; Feng, D.; Wei, F.; Zhang, J.; De Clercq, E.; Pannecouque, C.; Chen, C. H.; Lee, K. H.; Murugan, N.; Steitz, T.; Zhan, P.; Liu, X. Identification of dihydrofuro[3,4-*d*]pyrimidine derivatives as novel HIV-1 non-nucleoside reverse transcriptase inhibitors with promising antiviral activities and desirable physicochemical properties. *J. Med. Chem.* **2019,** 62, 1484-1501.

8. Rotili, D.; Tarantino, D.; Nawrozkij, M. B.; Babushkin, A. S.; Botta, G.; Marrocco, B.; Cirilli, R.; Menta, S.; Badia, R.; Crespan, E.; Ballante, F.; Ragno, R.; Este, J. A.; Maga, G.; Mai, A. Exploring the role of 2-chloro-6-fluoro substitution in 2-alkylthio-6-benzyl-5-alkylpyrimidin-4(3H)-ones: effects in HIV-1-infected cells and in HIV-1 reverse transcriptase enzymes. *J. Med. Chem.* **2014,** 57, 5212-5225.

9. Li, A.; Ouyang, Y.; Wang, Z.; Cao, Y.; Liu, X.; Ran, L.; Li, C.; Li, L.; Zhang, L.; Qiao, K.; Xu, W.; Huang, Y.; Zhang, Z.; Tian, C.; Liu, Z.; Jiang, S.; Shao, Y.; Du, Y.; Ma, L.; Wang, X.; Liu, J. Novel pyridinone derivatives as non-nucleoside reverse transcriptase inhibitors (NNRTIs) with high potency against NNRTI-resistant HIV-1 strains. *J. Med. Chem.* **2013,** 56, 3593-3608.

10. Zhao, T.; Meng, Q.; Kang, D.; Ji, J.; De Clercq, E.; Pannecouque, C.; Liu, X.; Zhan, P. Discovery of novel indolylarylsulfones as potent HIV-1 NNRTIs via structure-guided scaffold morphing. *Eur. J. Med. Chem.* **2019,** 182, 111619.

11. Wainberg, M. A.; Zaharatos, G. J.; Brenner, B. G. Development of antiretroviral drug resistance. *N. Engl. J. Med.* **2011,** 365, 637-646.

12. Wang, Y.; De Clercq, E.; Li, G. Current and emerging non-nucleoside reverse transcriptase inhibitors (NNRTIs) for HIV-1 treatment. *Expert Opin. Metab. Toxicol.* **2019**, 15, 813-829.

13. Kang, D.; Fang, Z.; Li, Z.; Huang, B.; Zhang, H.; Lu, X.; Xu, H.; Zhou, Z.; Ding, X.; Daelemans, D.; De Clercq, E.; Pannecouque, C.; Zhan, P.; Liu, X. Design, synthesis, and evaluation of thiophene[3,2-*d*]pyrimidine derivatives as HIV-1 non-nucleoside reverse transcriptase inhibitors with significantly improved drug resistance profiles. *J. Med. Chem.* **2016,** 59, 7991-8007.

14. Kang, D.; Fang, Z.; Huang, B.; Lu, X.; Zhang, H.; Xu, H.; Huo, Z.; Zhou, Z.; Yu, Z.; Meng, Q.; Wu, G.; Ding, X.; Tian, Y.; Daelemans, D.; De Clercq, E.; Pannecouque, C.; Zhan, P.; Liu, X. Structure-based optimization of thiophene[3,2-*d*]pyrimidine derivatives as potent HIV-1 non-nucleoside reverse transcriptase inhibitors with improved potency against resistance-associated variants. *J. Med. Chem.* **2017,** 60, 4424-4443.

15. Yang, Y.; Kang, D.; Nguyen, L. A.; Smithline, Z. B.; Pannecouque, C.; Zhan, P.; Liu, X.; Steitz,

T. A. Structural basis for potent and broad inhibition of HIV-1 RT by thiophene[3,2-*d*]pyrimidine non-nucleoside inhibitors. *eLife* **2018,** 7, pii: e36340.

16. Zhou, Z.; Liu, T.; Wu, G.; Kang, D.; Fu, Z.; Wang, Z.; De Clercq, E.; Pannecouque, C.; Zhan, P.; Liu, X. Targeting the hydrophobic channel of NNIBP: discovery of novel 1,2,3-triazole-derived diarylpyrimidines as novel HIV-1 NNRTIs with high potency against wild-type and K103N mutant virus. *Org. Biomol. Chem.* **2019,** 17, 3202-3217.

17. Huo, Z.; Zhang, H.; Kang, D.; Zhou, Z.; Wu, G.; Desta, S.; Zuo, X.; Wang, Z.; Jing, L.; Ding, X.; Daelemans, D.; De Clercq, E.; Pannecouque, C.; Zhan, P.; Liu, X. Discovery of novel diarylpyrimidine derivatives as potent HIV-1 NNRTIs targeting the "NNRTI adjacent" binding site. *ACS Med. Chem. Lett.* **2018,** 9, 334-338.

18. Jiang, X.; Yu, J.; Zhou, Z.; Kongsted, J.; Song, Y.; Pannecouque, C.; De Clercq, E.; Kang, D.; Poongavanam, V.; Liu, X.; Zhan, P. Molecular design opportunities presented by solvent-exposed regions of target proteins. *Med. Res. Rev.* **2019,** 39, 2194-2238.

19. Carroll, S. S.; Olsen, D. B.; Bennett, C. D.; Gotlib, L.; Graham, D. J.; Condra, J. H.; Stern, A. M.; Shafer, J. A.; Kuo, L. C. Inhibition of HIV-1 reverse transcriptase by pyridinone derivatives. Potency, binding characteristics, and effect of template sequence. *J. Biolo. Chem.* **1993,** 268, 276-281.

20. Kanayama, N.; Kanari, C.; Masuda, Y.; Ohmori, S.; Ooie, T. Drug-drug interactions in the metabolism of imidafenacin: role of the human cytochrome P450 enzymes and UDP-glucuronic acid transferases, and potential of imidafenacin to inhibit human cytochrome P450 enzymes. *Xenobiotica* **2007,** 37, 139-154.

21. Kang, D.; Huo, Z.; Wu, G.; Xu, J.; Zhan, P.; Liu, X. Novel fused pyrimidine and isoquinoline derivatives as potent HIV-1 NNRTIs: a patent evaluation of WO2016105532A1, WO2016105534A1 and WO2016105564A1. *Expert Opin. Ther. Pat.* **2017,** 27, 383-391.

22. Shamovsky, I.; Connolly, S.; David, L.; Ivanova, S.; Norden, B.; Springthorpe, B.; Urbahns, K. Overcoming undesirable HERG potency of chemokine receptor antagonists using baseline lipophilicity relationships. *J. Med. Chem.* **2008,** 51, 1162-1178.

23. Pannecouque, C.; Daelemans, D.; De Clercq, E. Tetrazolium-based colorimetric assay for the detection of HIV replication inhibitors: revisited 20 years later. *Nat. Protoc.* **2008,** 3, 427-434.

24. Hombrouck, A.; Voet, A.; Van Remoortel, B.; Desadeleer, C.; De Maeyer, M.; Debyser, Z.; Witvrouw, M. Mutations in human immunodeficiency virus type 1 integrase confer resistance to the naphthyridine L-870,810 and cross-resistance to the clinical trial drug GS-9137. *Antimicrob. Agents Chemother.* **2008,** 52, 2069-2078.

25. Snoeck, J.; Riva, C.; Steegen, K.; Schrooten, Y.; Maes, B.; Vergne, L.; Van Laethem, K.; Peeters, M.; Vandamme, A. M. Optimization of a genotypic assay applicable to all human immunodeficiency virus type 1 protease and reverse transcriptase subtypes. *J. Virolo. Methods,* **2005,** 128, 47-53.

26. Vrancken, B.; Trovao, N. S.; Baele, G.; van Wijngaerden, E.; Vandamme, A. M.; van Laethem, K.; Lemey, P. Quantifying next generation sequencing sample pre-processing bias in HIV-1 complete genome sequencing. *Viruses* **2016,** 8, pii: E12.

27. Suzuki, K.; Craddock, B. P.; Okamoto, N.; Kano, T.; Steigbigel, R. T. Poly A-linked colorimetric microtiter plate assay for HIV reverse transcriptase. *J. Virolo. Methods,* **1993,** 44, 189-198.

28. Katchman, A. N.; Koerner, J.; Tosaka, T.; Woosley, R. L.; Ebert, S. N. Comparative evaluation of HERG currents and QT intervals following challenge with suspected torsadogenic and nontorsadogenic drugs. *J. Pharmacolo. Exp. Ther.* **2006,** 316, 1098-1106.

## Table of Contents graphic

**$EC_{50}$ (nM) =**
3.24 (WT);
2.05 (L100I);
2.34 (K103N);
6.57 (Y181C);
7.59 (Y188L);
6.70 (E138K);
4.81 (F227L+V106A);
5.45 (K103N+Y181C);
**$CC_{50}$ =** 10100 nM

Improved Drug Resistance Profiles

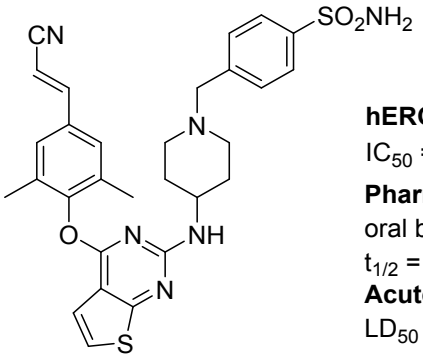


**9a**

**hERG Inhibitory Activity**
$IC_{50}$ =0.979 μM
**Pharmacokinetics**
oral bioavailability ***F*** **= 37.06 %**
$t_{1/2}$ = 2.8 h (po)
**Acute Toxicity**
$LD_{50}$ > 2000 mg/kg

Favorable Pharmacokinetic Properties